RESEARCH PAPER

Synergistic effect of Zinc Phthalocyanine (ZnPC)@MIL-101 framework and laser radiation on mcf-7 breast cancer cells: an experimental combination study

*Mahin Velayati[1, 2], Zahra Sabouri[2, 3], Ramin Rezaee[1], Mohammad Hasan Soheilifar[4], Hoda Keshmiri Neghab[4], Samaneh Hashemi Ghoochani[3], Alireza Hashemzadeh[3], Majid Darroudi[5]**

[1] Applied Biomedical Research Center, Mashhad University of Medical Sciences, Mashhad, Iran
[2] Student Research Committee, Mashhad University of Medical Sciences, Mashhad, Iran
[3] Department of Medical Biotechnology and Nanotechnology, Faculty of Medicine, Mashhad University of Medical Sciences, Mashhad, Iran
[4] Department of Medical Laser, Medical Laser Research Center, Yara Institute, ACECR, Tehran, Iran
[5] Nuclear Medicine Research Center, Mashhad University of Medical Sciences, Mashhad, Iran

ABSTRACT

Objective(s): Zinc phthalocyanine (ZnPC), a potent photosensitizer for photodynamic therapy (PDT), often suffers from poor solubility and aggregation, limiting its efficacy. Metal-organic frameworks (MOFs) like MIL-101 can serve as nanocarriers to overcome these issues. This experimental study investigates the synthesis, characterization, and synergistic anticancer efficacy of ZnPC incorporated within the MIL-101 framework (ZnPC@MIL-101) against MCF-7 breast cancer cells. ZnPC was chosen for its strong red-light absorption and high reactive oxygen species (ROS) generation, while MIL-101 offers a stable, porous platform to enhance ZnPC delivery and photoactivity.

Materials and Methods: ZnPC@MIL-101 (Cr) was synthesized via a double-solvent method. Characterization involved PXRD, BET analysis, FESEM, DLS, EDX spectroscopy, and UV-Vis spectroscopy. The loading capacity was determined, and singlet oxygen generation was quantified. Anticancer efficacy and PDT synergy with 660 nm laser radiation were evaluated on MCF-7 cells using MTT assays. Statistical analysis was performed using ANOVA.

Result: Successful synthesis of crystalline ZnPC@MIL-101 was confirmed. The loading capacity of ZnPC was found to be 8.5%. BET analysis showed reduced surface area (1709.4 m^2/g) and pore size (1.71 nm) post-ZnPC loading, indicating effective incorporation. FESEM/DLS showed particle sizes around 368/439.7 nm, respectively. EDX confirmed uniform Zn distribution. The UV-Vis spectrum of ZnPC@MIL-101 displayed the characteristic Q-band of ZnPC, and the nanocomposite exhibited significant singlet oxygen generation upon laser irradiation. ZnPC@MIL-101 exhibited moderate dark toxicity (IC_{50}: 25 µg/mL), which was significantly enhanced upon laser irradiation (IC_{50}: 10 µg/mL, $p < 0.01$).

Conclusion: ZnPC@MIL-101 combined with laser radiation demonstrated a significant synergistic reduction in MCF-7 cell viability. This highlights its potential as an effective PDT agent, offering a promising strategy to enhance ZnPC-based cancer treatment.

Keywords: *Metal-Organic frameworks; Photosensitizing agents; Drug delivery; Nanocarrier; Cytotoxicity.*

How to cite this article
Velayati M, Sabouri Z, Rezaee R, Soheilifar MH, Keshmiri Neghab H, Hashemi Ghoochani S, Hashemzadeh A, Darroudi M. Synergistic effect of zinc phthalocyanine (ZnPC)@MIL-101 framework and laser radiation on mcf-7 breast cancer cells: an experimental combination study. Nanomed J. 2026; 13(2): 296-309. DOI: 10.22038/NMJ.2026.89968.2274

INTRODUCTION

Photodynamic therapy (PDT) is a minimally invasive treatment that requires administering a photosensitizing agent and subsequently activating it with specific wavelength light, usually in an oxygen-rich environment [1]. Upon light irradiation, the PS generates reactive oxygen species (ROS), primarily singlet oxygen, which induce oxidative damage to cellular components, leading to cell death in targeted tissues like cancer cells [2]. Breast cancer is one of the most commonly diagnosed cancers and a leading cause of cancer-

* *Corresponding author:* Majid Darroudi, Assistant Professor, Nuclear Medicine Research Center, Mashhad University of Medical Sciences, Mashhad, Iran. E-Mail address: darroudim@mums.ac.ir.
Note. This manuscript was submitted on July 27, 2025; approved on November 26, 2025.
© 2026. This work is openly licensed via CC BY 4.0. This is an Open Access article distributed under the terms of the Creative Commons Attribution License (https://creativecommons.org/licenses), which permits unrestricted use, distribution, and reproduction in any medium, provided the original work is properly cited.

related mortality in women globally, necessitating the development of more effective and less toxic treatment strategies [3-6].

The unique characteristics of metal-organic frameworks (MOFs), like tunable porosity, high surface area, and biocompatibility, have made them a subject of great interest for various biomedical applications, including their use as carriers in photodynamic therapy [7, 8]. Integrating therapeutic molecules into MOFs can enhance their delivery, stability, and efficacy, making them a promising platform for cancer treatment [9, 10]. Among the numerous MOFs, MIL-101, a chromium-based MOF, has emerged as a prominent candidate for such applications because of its exceptionally large surface area, robust and stable porous structure, which makes it an ideal carrier for therapeutic agents [11, 12].

Zinc phthalocyanine (ZnPC) is a well-established second-generation photosensitizer frequently employed in PDT [13-15]. It exhibits strong absorption in the red region of the light spectrum (Q-band, typically 670-680 nm), which allows for deeper tissue penetration of activating light compared to PS absorbing at shorter wavelengths [16, 17]. Furthermore, ZnPC is known for its high ROS generation efficiency and relatively low dark toxicity [18]. However, the clinical application of free ZnPC is often hindered by its poor aqueous solubility and strong tendency to aggregate in biological environments; aggregation can quench its photoactivity and significantly reduce its therapeutic efficacy [19, 20].

To overcome these limitations, various nanocarrier systems have been developed for ZnPC. Encapsulating ZnPC within MOFs such as MIL-101 (forming ZnPC@MIL-101) is a strategy to improve its dispersibility, prevent aggregation, and maintain its monomeric, photoactive state [21-23]. The large pore volume and high surface area of MIL-101 are expected to facilitate efficient loading and stabilization of ZnPC molecules [21]. Moreover, the robust framework of MIL-101 can protect the encapsulated ZnPC from premature degradation and can enhance its accumulation at the tumor site, often through passive targeting via the Enhanced Permeability and Retention (EPR) effect common to nanosized drug delivery systems [24, 25]**.** Such integration is anticipated not only to improve the bioavailability of ZnPC but also to enhance its overall photodynamic activity [26-28]. Indeed, studies have demonstrated that MOF-based delivery systems can enhance the photodynamic activity of various photosensitizers, including porphyrins and phthalocyanines, by improving their solubility, cellular uptake, and ROS generation capabilities [23, 29-31]**.** For example, a study by Ghoochani *et al*. (10) explored Zn(II) porphyrin encapsulated in MIL-101 for the PDT of breast cancer cells, underscoring the potential of MIL-101 as a nanocarrier in this context [32]**.**

The novelty of the present study lies in the synthesis, detailed physicochemical and photophysical characterization, and in vitro evaluation of the synergistic anticancer efficacy of ZnPC specifically incorporated within the MIL-101(Cr) framework when combined with laser radiation against MCF-7 human breast cancer cells. While MOFs have been explored as drug carriers, this work provides a focused investigation into the ZnPC@MIL-101 (Cr) system, quantifying its drug loading, singlet oxygen generation, and demonstrating a statistically significant, dose-dependent synergistic phototoxic effect in a relevant breast cancer model. MCF-7 cells were chosen as a well-established and commonly used human breast adenocarcinoma cell line, representing estrogen receptor-positive breast cancer, to evaluate the potential of ZnPC@MIL-101 in a relevant cancer model [23, 25, 33-35]. This study aims to elucidate the potential of this specific nanocomposite system to improve ZnPC-mediated PDT outcomes.

MATERIALS AND METHODS

Equipment and reagents

All chemicals were sourced from Sigma and Merck Co.

Characterization methods

The synthesized materials were characterized using various analytical techniques. A Fourier Transform Infrared Spectrometer (FTIR; Shimadzu-8400, Japan) was used to identify functional groups. Powder X-ray Diffraction (PXRD; Philips, Netherlands) was employed to determine the crystalline structure and phase purity of the samples. The crystallite size (D) was estimated from the PXRD data using the Scherrer equation: $D = K\lambda / (\beta \cos\theta)$, where K is the shape factor (0.9), λ is the X-ray wavelength (0.154 nm), β is the full width at half maximum (FWHM) of the diffraction peak in radians, and θ is the Bragg angle**.** The surface area and pore characteristics were analyzed using BET analysis (BELSORP Mini II, Microtrac MRB, Japan) via N2 adsorption-desorption isotherms. The morphology and particle size of the materials were observed using a FESEM (Hitachi S-4800, Japan), which was also equipped for EDX spectroscopy to determine elemental composition and distribution.

DLS (Malvern Zetasizer Nano ZS, UK) was used to measure the hydrodynamic size (Z-Average, reported as an intensity-weighted mean) and polydispersity index (PI) of the particles in suspension. UV-Visible (Shimadzu UV-2600 spectrophotometer) absorption spectra were recorded to confirm the incorporation of ZnPC.

Preparation of MIL-101

The synthesis of MIL-101 was initiated by combining $Cr(NO_3)_3{\cdot}9H_2O$ (4.0 g, 10.0 mmol), terephthalic acid ($C_8H_6O_4$) (1.66 g, 10.0 mmol), and deionized water (40 mL) in an autoclave. This mixture was then subjected to hydrothermal conditions by heating it to 218 ˚C for 18 h, allowing the formation of the MIL-101 framework. After the reaction, the resulting precipitates were carefully separated from the mixture [36]. These precipitates were then immersed in N, N-dimethylformamide (C_3H_7NO) (40 mL) and maintained at 70 °C for 8 h to facilitate the removal of any unreacted organic linkers and impurities. Subsequently, the product was washed multiple times with water, acetone (C_3H_6O), and methanol to ensure purity. In the end, the purified product was dried at 25 °C, resulting in the formation of MIL-101.

Preparation of ZnPc@MIL-101(Cr)

Synthesis of ZnPc@MIL-101(Cr) was initiated by incorporating Zn^{2+} ions into the pores of MIL-101(Cr) using a double-solvent process [37]. This method involves distinct roles for each solvent: dry n-hexane serves as a non-polar medium to ensure good dispersion of the activated MIL-101(Cr) and facilitate the initial even distribution and adsorption of $ZnCl_2$ onto the framework surfaces and into the pore entrances, while ethanol is subsequently used as a polar solvent for efficiently dissolving and mixing the Zn@MIL-101(Cr) complex with phthalonitrile before the cyclization reaction in DES. Initially, activated MIL-101 (Cr, 200 mg) was added to dry n-hexane (40 mL) and stirred for 30 min. This step ensures that the MIL-101(Cr) particles are well-dispersed in the solvent, facilitating the subsequent loading of Zn^{2+} ions. Subsequently, a solution of $ZnCl_2$ (0.123 mL, 1 M) was added dropwise under stirring. The dropwise addition allows for the gradual incorporation of Zn^{2+} ions in the MIL-101, preventing agglomeration and ensuring uniform distribution. The mixture was continuously stirred for 3 h to allow sufficient time for the Zn^{2+} ions to penetrate the pores of MIL-101 (Cr). After this period, the powder was filtered and dried at 130 °C for 12 h to remove residual solvents and stabilize the Zn@MIL-101(Cr) complex. For the synthesis of ZnPc@MIL-101(Cr), 200 mg of the dried Zn@MIL-101(Cr) was combined with 2 mL of ethanol and briefly sonicated to ensure thorough mixing [37]. Phthalonitrile (0.492 mmol) was then added to it and stirred for 60 min to facilitate the formation of the phthalocyanine complex. Following this, ethanol was removed to concentrate the reaction mixture, and 2 mL of DES (Deep Eutectic Solvent) was added to the remaining solid. The mixture was then placed at 150 °C/30 min, forming ZnPc@MIL-101(Cr), as indicated by the deep blue color of the as-prepared sample. This heating step promotes the cyclization of phthalonitrile to form the phthalocyanine ring structure, which coordinates with the Zn^{2+} ions within the MIL-101(Cr) framework. The synthesized nanovehicle was subsequently dried and activated at 150 °C overnight to remove any remaining solvents and enhance the stability and activity of ZnPc@MIL-101(Cr) before cancer treatment.

Cell culture and preparation

In the initial stage of cell culture, MCF-7 human breast adenocarcinoma cells were obtained from the Pasteur Institute (Tehran, Iran). The cells were cultured in Dulbecco's Modified Eagle Medium (DMEM) supplemented with 10% Fetal Bovine Serum (FBS), penicillin (100 IU/mL), and streptomycin (100 µg/mL). Cultivation was carried out in a humidified incubator at 37 °C with an atmosphere of 5% CO_2. For subculturing and experiments, cells were detached using a 0.025% trypsin-0.02% EDTA solution and washed with phosphate-buffered saline (PBS).

Determination of encapsulation efficiency and loading capacity

The amount of ZnPC loaded into MIL-101 was determined by UV-Vis spectroscopy. A known amount of ZnPC@MIL-101 was dissolved in dimethylformamide (DMF) to release the encapsulated ZnPC. The concentration of ZnPC was then measured by recording the absorbance at its characteristic Q-band peak (λmax ≈ 670 nm) and comparing it to a standard calibration curve of free ZnPC in DMF. The loading capacity (LC) was calculated using the following formula:

LC (%) = (Weight of loaded ZnPC / Weight of ZnPC@MIL-101) × 100%

Singlet oxygen generation assay

The generation of singlet oxygen ($^1O_2$) by ZnPC@MIL-101 upon irradiation was detected chemically using 1,3-diphenylisobenzofuran (DPBF) as a probe. DPBF reacts with $^1O_2$, leading to a

decrease in its absorbance at 415 nm. In a typical experiment, a solution of ZnPC@MIL-101 and DPBF in DMF was irradiated with a 660 nm laser (2 J/cm²). The absorbance of DPBF at 415 nm was monitored at regular intervals using a UV-Vis spectrophotometer. A solution containing only DPBF was used as a negative control.

Cell proliferation assay

The assessment of cell proliferation was conducted utilizing the MTT assay, which measures cellular metabolic activity as an indicator of viability. MCF-7 cells were plated into 96-well plates at a density of approximately 8×10^4 cells/well and allowed to adhere for 24 h. Following this period, cells were treated with the test compounds as described for the photodynamic treatment evaluation. After the respective incubation and/or irradiation procedures, 10 µL of MTT solution (5 mg/mL) was added to each well, and the plates were incubated for an additional 4 h. Afterward, 100 µL of Dimethyl Sulfoxide was added to each well to dissolve the formazan crystals formed by metabolically active cells. The absorbance was measured at 570 nm with a reference wavelength of 630 nm using an ELISA plate reader. Cell survival rates were expressed as a percentage of the untreated control. Each experiment was performed in triplicate. IC_{50} values (the concentration of compound required to inhibit cell growth by 50%) were calculated from the dose-response curves.

Photodynamic treatment evaluation

For photodynamic treatment evaluation, two main experimental conditions were established: (1) incubation with compounds in darkness (Dark group) and (2) incubation followed by laser exposure (Treatment group). MCF-7 breast cancer cells were incubated with varying concentrations (0-100 µg/mL) of MIL-101 or ZnPC@MIL-101 for 24 h in darkness. For the Treatment group, after the 24 h incubation and replacement of the medium with fresh medium, cells were exposed to a 660 nm diode laser (continuous wave) at an energy density of 2 J/cm². The laser power output was adjusted to deliver this energy density over the calculated exposure time. The impact on cell viability was also specifically assessed using the determined IC_{50} concentrations of ZnPC@MIL-101: 25 µg/mL for the dark condition and 10 µg/mL for the laser-irradiated condition. The cellular uptake of nanoparticles was qualitatively inferred from the observed phototoxicity. The 24-hour incubation period was selected based on common protocols, allowing sufficient time for particle-cell interaction and internalization in PDT studies [38].

Statistical analysis

Quantitative results from cell proliferation assays are displayed as the mean ± standard deviation (SD), derived from a minimum of three separate experiments. To assess statistical significance across groups, a one-way ANOVA was employed, complemented by Tukey's post-hoc test for multiple comparisons, with a p-value below 0.05 denoting statistical significance. The IC_{50} values were calculated by applying a sigmoidal curve model to the dose-response data within GraphPad Prism software.

RESULTS

PXRD pattern

The PXRD patterns depicted in Fig. 1 provide valuable insights into the crystal structure of ZnPC@MIL-101. The black line represents the simulated PXRD pattern for MIL-101. Notably, this pattern exhibits several sharp peaks, indicative of a well-defined crystalline structure. The diffraction angle (2θ) values range from 5 to 80°. The green line corresponds to the experimental PXRD pattern of ZnPC@MIL-101. Remarkably, this pattern closely aligns with the simulated MIL-101 pattern, with minor variations. This alignment suggests that ZnPC@MIL-101 retains the crystalline structure of MIL-101. The agreement between the experimental and simulated patterns supports the successful synthesis of ZnPC@MIL-101.

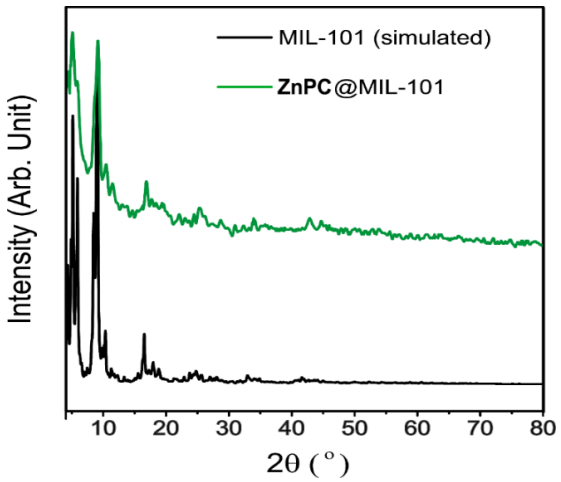

Fig. 1. PXRD pattern of ZnPC@MIL-101 vs. simulated pattern.

Furthermore, the close match between the two patterns implies phase purity, indicating that

ZnPC@MIL-101 predominantly consists of the desired crystalline phase. The major peaks are indexed with their Miller indices ((111), (220), (311), (400), (511), (531), (822), and (753)), confirming the crystalline structure of the MIL-101. The crystallite size of ZnPC@MIL-101 was determined using the Scherrer equation. The calculated crystallite size is 47.91 nm, providing valuable information about the material's nanostructure. In summary, the PXRD data confirm the successful synthesis of ZnPC@MIL-101, its phase purity, and its structural compatibility with MIL-101.

Surface area and pore characteristics

The BET analysis provides critical insights into the materials' surface area and pore structure. In our study, we investigated two materials: MIL-101 and ZnPC@MIL-101 (Fig. 2).

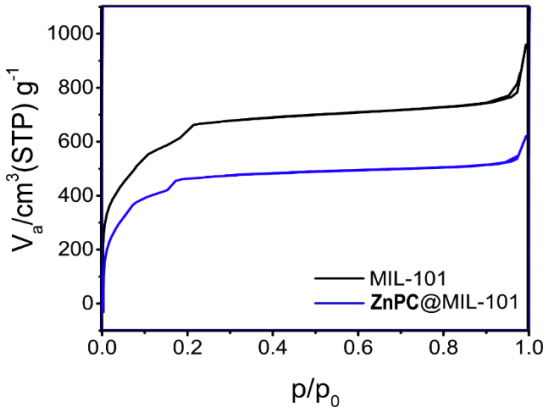

Fig. 2. BET analysis of MIL-101 and ZnPC@MIL-101.

The specific surface area, determined through N2 adsorption-desorption isotherms, revealed that MIL-101 exhibited a surface area of 2282.9 m²/g. At the same time, ZnPC@MIL-101 had a decreased surface area of 1709.4 m²/g. Notably, after loading with ZnPC, the BET surface area decreased by 573.5 m²/g. This reduction suggests that the ZnPC molecules were effectively immobilized within the pores of MIL-101, leading to a structural integration. Beyond surface area, pore size is a crucial parameter. Our results indicated a significant decrease in pore size from 2.52 nm for MIL-101 to 1.71 nm for ZnPC@MIL-101 upon ZnPC loading. This reduction in pore diameter further supports the hypothesis that ZnPC molecules penetrated the pores and became an integral part of the material's structure. Additionally, the total pore volume decreased from 1.44 cm³/g for MIL-101 to 0.94 cm³/g for ZnPC@MIL-101, representing a 35% reduction. These findings underscore the successful functionalization of ZnPC@MIL-101 and confirm the impregnation method's efficacy in introducing ZnPC into the porous framework.

Morphology and particle size

The FESEM images provide valuable insights into the structural characteristics of these materials (Fig. 3). The distinct morphologies impact surface area, porosity, and reactivity. In MIL-101, we observe a heterogeneous arrangement of octahedral and polyhedral crystals. These crystals exhibit well-defined edges and smooth faces, suggesting a high-quality structure. Zooming in, individual octahedral crystals with sharp vertices become apparent, contributing to the overall surface area. The minimal surface defects enhance the material's integrity. In contrast, ZnPC@MIL-101 displays polyhedral structures, albeit less well-defined than MIL-101. The surfaces appear rougher, likely due to the incorporation of ZnPC molecules. This roughness could enhance adsorption properties or catalytic activity. Closer examination reveals surface texture differences, indicating successful integration of ZnPC into the MIL-101 framework. The FESEM images (Fig. 3c, d) suggest a generally uniform contribution of MIL-101 as the structural base with ZnPC influencing the surface texture rather than forming distinct, separate agglomerates. This is further supported by EDX elemental mapping (Fig. 6a, b), which shows a diffuse, widespread distribution of zinc, indicating that ZnPC is incorporated throughout the MIL-101 matrix rather than existing as large, separate clusters. This homogenous incorporation is beneficial for consistent photodynamic activity throughout the nanoparticle. Similar morphological analyses confirming MOF integrity after photosensitizer loading have been documented for ZIF-8 frameworks used in PDT [39].

The particle size distribution obtained from FESEM analysis of MIL-101 shows a peak frequency within the range of approximately 200–400 nm (mean size 395.50 nm) (Fig. 4). This suggests that MIL-101 primarily consists of particles falling within this size range. Similarly, the particle size distribution for ZnPC@MIL-101 exhibits a peak frequency in the same 200–400 nm range. However, compared to MIL-101, ZnPC@MIL-101 has a narrower distribution, with a mean particle size of 368.07 nm. The observed decrease in mean particle size for ZnPC@MIL-101 suggests that the encapsulation or combination process involved in creating ZnPC@MIL-101 may influence the final particle dimensions compared to MIL-101 alone.

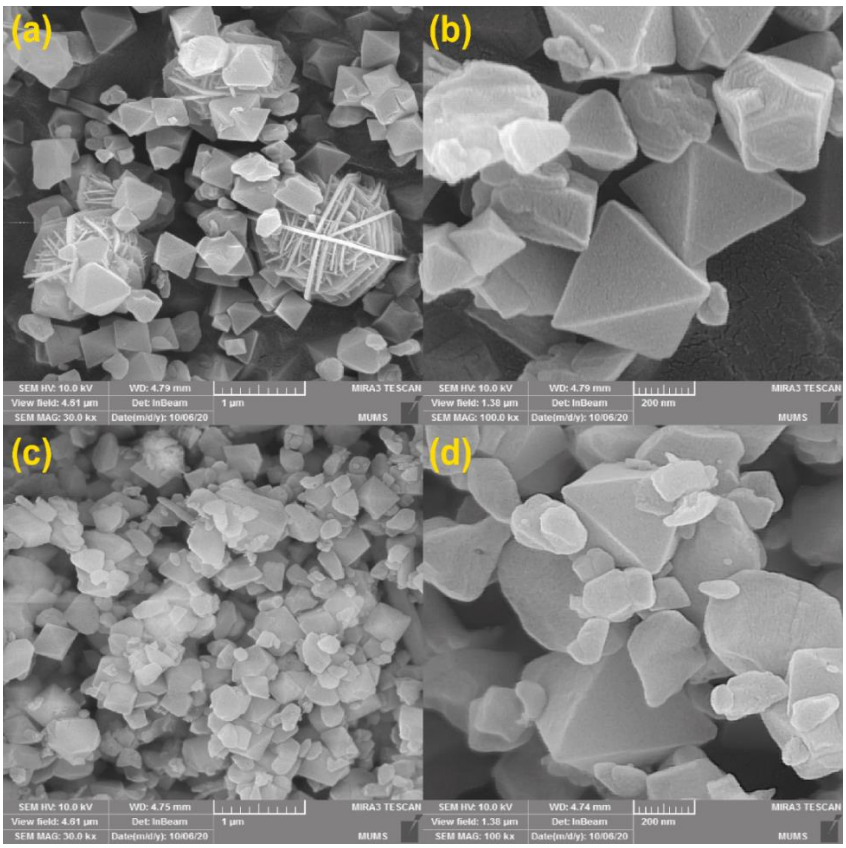

Fig. 3. FESEM of MIL-101 (a, b) and ZnPC@MIL-101 (c, d). Image (a) shows larger octahedral crystals of MIL-101, while (b) is a magnified view showing well-defined crystal faces. Image (c) depicts the polyhedral structure of ZnPC@MIL-101 with a rougher surface, and (d) offers a closer look at this altered morphology due to ZnPC incorporation.

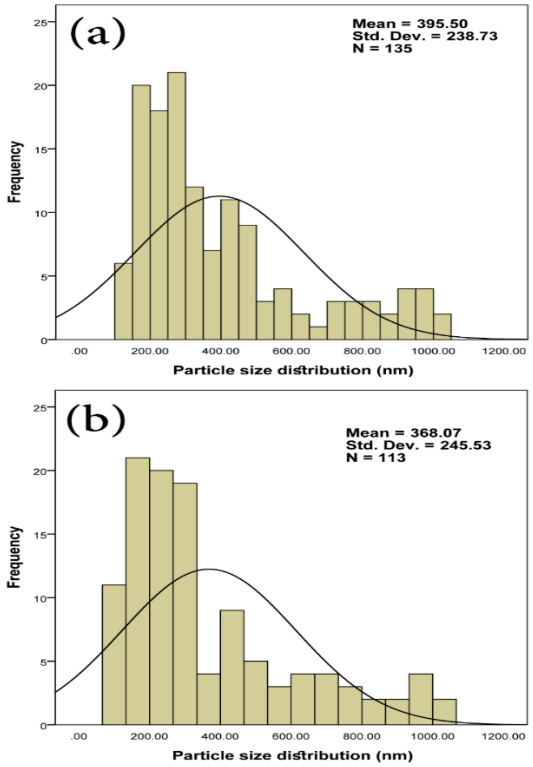

Fig. 4. Particle size distribution histograms obtained from FESEM images of MIL-101 (a) and ZnPC@MIL-101 (b).

Understanding the difference between hydrodynamic and solid phase sizes is crucial for interpreting Dynamic Light Scattering (DLS) data. The hydrodynamic size provides insight into how the particles will behave in a fluid environment, which is essential for applications where the particles are used in solution. On the other hand, the solid phase size gives information about the intrinsic properties of the particles themselves. ZnPC@Mil-101, where ZnPC is integrated with the MIL-101, has shown a pronounced peak in the DLS measurement (intensity-weighted distribution), signifying that most particles cluster around a specific diameter. The Z-Average (mean diameter) is precisely 439.7 nm (Fig. 5). Additionally, the Polydispersity Index (PI) stands at 0.491, indicating a relatively narrow size distribution within the sample. The hydrodynamic size is typically more prominent than the solid phase size due to the solvent layer and interactions in the fluid medium. The EDX analysis confirms the presence of carbon, nitrogen, oxygen, and zinc in ZnPC@MIL-101 (Fig. 6). Interestingly, the 3D distribution of zinc shows scattered bright specks throughout the material. Rather than forming large clusters, zinc is uniformly distributed in small quantities. This uniform elemental distribution, evident from EDX, complements the FESEM observations by suggesting homogenous incorporation of ZnPC throughout the MIL-101 framework rather than surface deposition or isolated clustering, which is beneficial for predictable drug loading and release characteristics. The BET and EDX data strongly suggest successful incorporation. Future work should quantify this encapsulation efficiency for a more complete assessment.

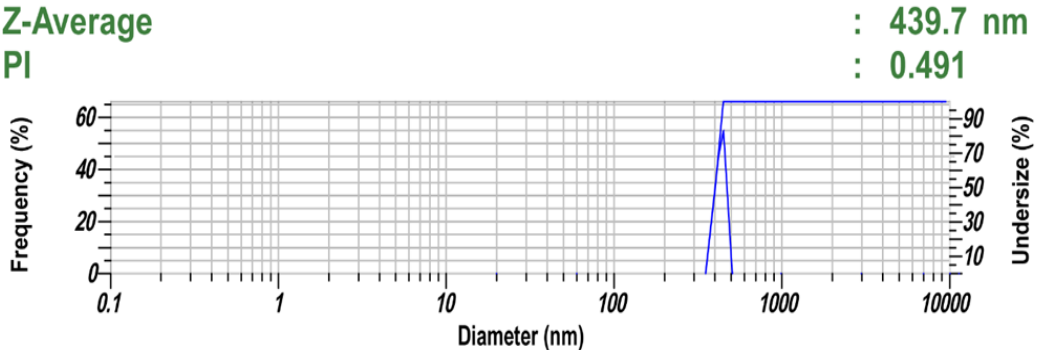

Fig. 5. DLS of ZnPC@MIL-101.

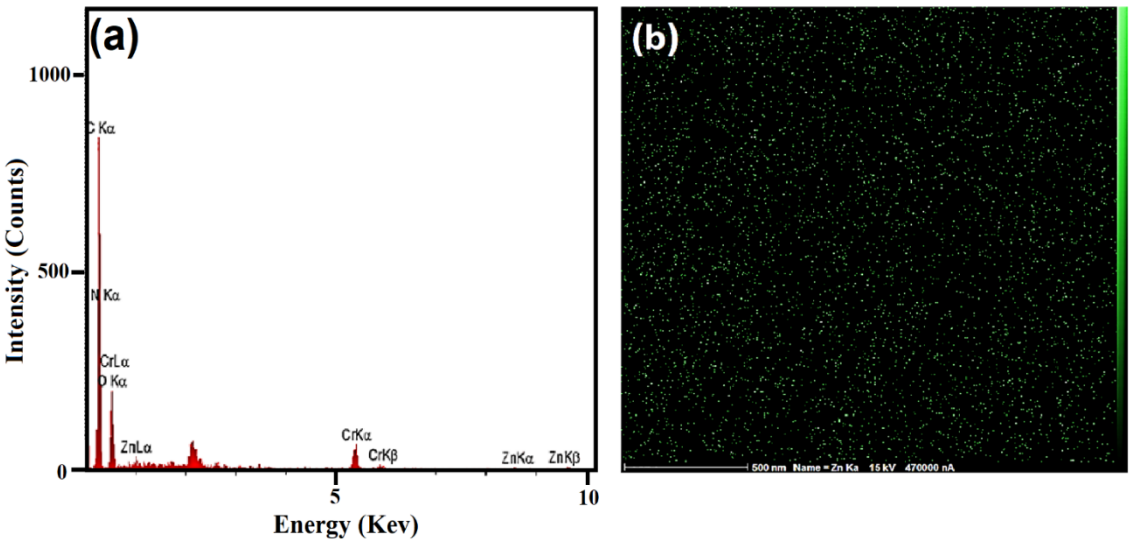

Fig. 6. The EDX analysis (a) spectrum of ZnPC@MIL-101 confirming elemental composition, and (b) elemental mapping showing the 3D distribution of Zinc in the sample.

Photophysical properties and ROS generation

The UV-Vis absorption spectra of Free ZnPC in DMF exhibit a sharp and intense Q-band absorption peak at approximately 670 nm, which is characteristic of its monomeric form. The spectrum of ZnPC@MIL-101 dispersed in DMF also shows this characteristic Q-band, confirming that ZnPC was successfully incorporated into the MIL-101 framework and retains its essential photophysical properties. The slight broadening of the peak in the nanocomposite suggests some interaction with the MOF structure, but critically, the absence of significant new peaks indicates that aggregation of ZnPC has been effectively prevented.

The ability of ZnPC@MIL-101 to generate singlet oxygen, the primary cytotoxic agent in PDT, was evaluated using DPBF as a chemical trap. The absorbance of DPBF at 415 nm decreased rapidly over time when mixed with ZnPC@MIL-101 and exposed to 660 nm laser light. In contrast, the control group containing only DPBF showed a negligible decrease in absorbance under the same irradiation conditions. This result clearly demonstrates that ZnPC@MIL-101 is highly effective at generating singlet oxygen upon light activation, a prerequisite for a successful PDT agent.

Encapsulation efficiency and loading capacity

The encapsulation of ZnPC within the MIL-101 framework was quantified using UV-Vis spectroscopy. Based on the standard calibration curve for ZnPC, the loading capacity was calculated to be 8.5%. This indicates a successful loading of the photosensitizer into the MOF nanocarrier, which is consistent with the changes observed in the BET analysis.

Cellular studies

The viability of MCF-7 cells after treatment with MIL-101 alone, both in dark conditions and with laser irradiation, is presented in Fig. 7. In the dark, MIL-101 exhibited a dose-dependent reduction in cell viability, with approximately 50% viability observed at 100 µg/mL. Laser irradiation (660 nm, 2 J/cm²) alone (0 µg/mL MIL-101, red bar) showed minimal effect on cell viability, which remained near 100%. When MIL-101 was combined with laser radiation, a further decrease in cell viability was observed at higher concentrations compared to MIL-101 in the dark, although this enhancement was not substantial across all concentrations.

Fig. 8 shows the effect of ZnPC@MIL-101 on MCF-7 cell viability. In dark conditions (striped bars), ZnPC@MIL-101 caused a dose-dependent decrease in cell viability, with an IC_{50} value determined to be 25 µg/mL. Upon laser irradiation (red bars), the cytotoxic effect of ZnPC@MIL-101 was significantly enhanced, resulting in a lower IC_{50} value of 10 µg/mL. This more than two-fold decrease in IC_{50} was statistically significant ($p < 0.01$). This indicates a synergistic effect between the ZnPC@MIL-101 nanocomposite and laser activation, leading to a more pronounced reduction in cancer cell viability compared to the nanocomposite alone or MIL-101 with laser irradiation.

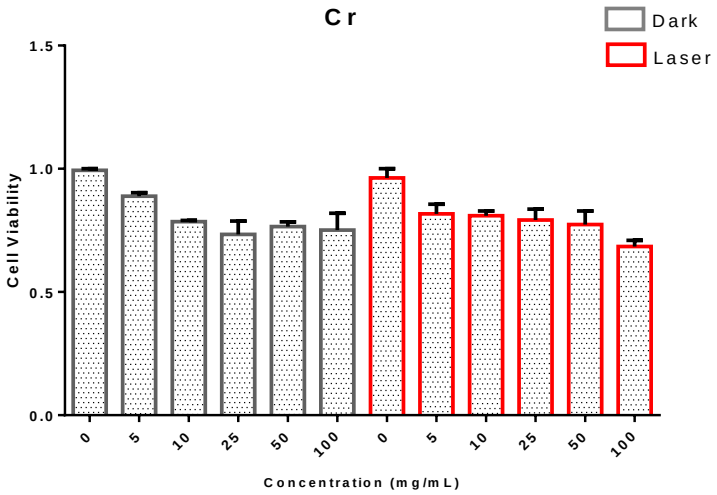

Fig. 7. The effect of different concentrations of MIL-101 on breast cancer MCF-7 cells after 24 h of incubation in the dark and then low-power laser radiation with a wavelength of 660 nm and an energy density of 2 J/cm². Data are presented as mean ± SD (n=3). $p < 0.01$ compared to the corresponding dark group.

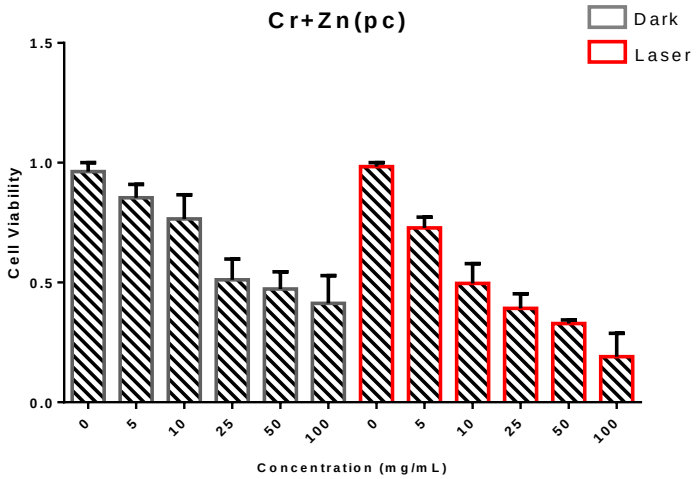

Fig. 8. The effect of different concentrations of ZnPC@MIL-101 combination on breast cancer MCF-7 cells after 24 h of incubation in the dark and then low-power laser irradiation with a wavelength of 660 nm and an energy density of 2 J/cm^2. Data are presented as mean ± SD (n=3). $p < 0.01$ compared to the corresponding dark group.

DISCUSSION

The successful development of a nanocarrier-based PDT agent relies on a thorough characterization of its physicochemical properties to ensure it can effectively deliver the photosensitizer and elicit a phototoxic response. In this study, we employed a suite of analytical techniques to validate the synthesis and properties of ZnPC@MIL-101. PXRD (Fig. 1) was essential to confirm that the crystalline structure of the MIL-101 framework was preserved after the incorporation of ZnPC, which is crucial for maintaining the stability and porous nature of the carrier. The BET analysis (Fig. 2) provided quantitative evidence of ZnPC loading by showing a significant reduction in surface area and pore volume, confirming that the photosensitizer molecules occupy the internal voids of the MOF. FESEM and DLS (Figs. 3-5) were used to determine the morphology and size distribution of the nanoparticles, which are critical parameters for their biological interactions and potential for passive tumor targeting via the EPR effect. Finally, EDX analysis (Fig. 6) confirmed the elemental composition and, importantly, the uniform distribution of zinc throughout the nanoparticles, suggesting a homogeneous loading of ZnPC rather than simple surface adsorption. Together, these characterizations provide a comprehensive picture of the ZnPC@MIL-101 nanocomposite and form the basis for interpreting its biological activity.

The primary goal of this research was to investigate the potential of a ZnPC@MIL-101 nanocomposite as an effective agent for the photodynamic therapy of MCF-7 breast cancer cells. ZnPC is a well-regarded photosensitizer due to its strong absorption in the 600-700 nm range (its Q-band) [40, 41], which aligns well with the 660 nm laser used in this study and allows for reasonable tissue penetration for PDT applications [42-46]. The photodynamic action of ZnPC is primarily mediated through the generation of singlet oxygen and other ROS upon light activation, leading to oxidative damage of cellular components and subsequent cell death, often via apoptosis or necrosis [18, 47]. While ZnPC can interact with cellular macromolecules like DNA [48] and proteins such as albumin (which influences its in vivo transport) [35, 49, 50]. Its therapeutic effect in PDT stems mainly from this ROS-mediated damage rather than specific molecular target binding in the manner of classical enzyme inhibitors or DNA intercalators.

A significant challenge with free ZnPC is its hydrophobicity and tendency to aggregate in aqueous physiological environments, which quenches its photoactivity [20, 51]. Nanocarriers like MOFs are employed to address these issues by improving solubility, preventing aggregation, and facilitating delivery [52-54]. MIL-101, with its high surface area and robust porous structure, is a suitable candidate [55]. Our synthesis of ZnPC@MIL-101, confirmed by PXRD retaining the MIL-101 crystallinity (Fig. 1), and the observed decrease in BET surface area and pore volume (Fig. 2), strongly suggests successful incorporation of ZnPC within the MOF framework. This encapsulation is crucial for maintaining ZnPC in a

monomeric, photoactive state, which is essential for efficient singlet oxygen generation [22, 23]. The FESEM and EDX analyses (Fig. 3, 6) further supported the formation of the nanocomposite with a fairly uniform distribution of Zn, indicating homogenous ZnPC loading rather than mere surface adsorption. This consistent distribution is vital for predictable photodynamic performance. Such loading has been shown in other MOF-PS systems to enhance PDT efficacy [39].

The cellular studies demonstrated a clear synergistic effect when ZnPC@MIL-101 was combined with laser irradiation (Fig. 8). The IC_{50} value for ZnPC@MIL-101 decreased from 25 µg/mL in the dark to 10 µg/mL upon laser activation. This enhanced phototoxicity is attributed to the efficient ROS generation by the MOF-encapsulated ZnPC. In contrast, while MIL-101 itself showed some dark cytotoxicity at higher concentrations (Fig. 7, IC_{50} > 100 µg/mL in dark), its combination with laser did not yield a comparable photodynamic enhancement, underscoring the critical role of ZnPC as the photosensitizer. It is noteworthy that MIL-101 in the dark at 100 µg/mL reduced cell viability to ~50%, whereas laser irradiation alone had a negligible effect. This inherent cytotoxicity of the MOF material at high concentrations must be considered when evaluating the net photodynamic effect. Such baseline toxicity of carrier materials is a known factor in nanomedicine. Comparing our findings with the literature, Ghoochani *et al*. [32] reported IC_{50} values of 14.3 µg/mL (light) and 81.6 µg/mL (dark) for Zn[TPP]@MIL-101 on MCF-7 cells. Our ZnPC@MIL-101 showed a dark IC_{50} of 25 µg/mL and a light IC_{50} of 10 µg/mL. The differences can be attributed to the type of photosensitizer (ZnPC vs. Zn [TPP]), loading efficiencies (our study found an 8.5% loading capacity), and potentially minor variations in experimental conditions. However, both studies highlight the utility of MIL-101 in enhancing the photodynamic effect of entrapped photosensitizers. Other studies employing ZnPC in different nanoformulations for MCF-7 cells have also reported significant PDT efficacy [34, 56-60], generally involving apoptotic cell death pathways triggered by caspase activation and mitochondrial dysfunction [57, 61, 62]. While the specific signaling pathways were not delineated here, such mechanisms are likely operative in the cell death observed with ZnPC@MIL-101-PDT. The results indicate that ZnPC@MIL-101 is a promising system for PDT. The MIL-101 framework likely improves ZnPC's dispersibility and prevents aggregation, thereby enhancing ROS generation upon irradiation. The observed synergistic effect confirms that the photodynamic action is the dominant mechanism for the enhanced cytotoxicity under laser light.

Potential Applications and Future Directions

The strengths of this study include the successful synthesis and thorough characterization of a ZnPC@MIL-101 nanocomposite and the demonstration of its synergistic photodynamic effect on MCF-7 breast cancer cells in vitro. The use of the well-established MIL-101 framework offers a stable and porous platform for ZnPC delivery, enhancing its photophysical properties by reducing aggregation, as confirmed by UV-Vis spectroscopy and singlet oxygen detection. The successful synthesis and characterization of ZnPC@MIL-101 and its demonstrated anticancer efficacy open up several potential applications and avenues for future research. The composite material's structural stability, high surface area, and effective photodynamic activity make it fit for biomedical applications comprising drug delivery and imaging. Further studies could explore optimizing ZnPC loading, quantifying encapsulation efficiency, and tuning the release kinetics. Assessment of ROS and singlet oxygen generation dosimetry, as well as photobleaching rates under therapeutic irradiation, would be essential for refining PDT protocols [16, 63]. Investigation into the cellular uptake mechanisms and quantification would also provide valuable insights. Additionally, the uniform distribution of ZnPC within the MIL-101 framework suggests that the composite could be used in other therapeutic contexts, such as antimicrobial treatments or environmental applications where photocatalytic activity is desired. Modifying the MIL-101 framework to incorporate different photosensitizers or functional molecules could further expand the material's versatility and range of applications. Furthermore, molecular modeling or simulation approaches, such as Density Functional Theory (DFT), as reported for other Zn-phthalocyanine systems [64], could be employed in future studies to theoretically investigate the electronic properties of ZnPC@MIL-101 and to better understand the interactions between the photosensitizer and the MOF framework, potentially guiding the design of even more effective PDT agents.

However, the study has several limitations. While we have now included foundational photophysical data, a more comprehensive photophysical characterization, including quantitative ROS/singlet oxygen dosimetry (crucial for understanding PDT efficiency) and

photobleaching rate determination (important for assessing sustained activity), was not performed. Cellular uptake was inferred from phototoxicity rather than directly quantified (e.g., by ICP-MS for zinc content or fluorescence microscopy of ZnPC). Additionally, the study was limited to a single breast cancer cell line (MCF-7) and did not explore the effects on normal, non-cancerous cells (to assess selectivity and potential for minimal side effects) or employ more complex in vitro models (e.g., 3D spheroids) or in vivo studies. These latter investigations are necessary to evaluate systemic toxicity, biodistribution, and true therapeutic potential in a more physiologically relevant context. These aspects were not explored in the current work primarily due to budgetary constraints and limitations in the available experimental setup.

CONCLUSION

In conclusion, this study successfully synthesized and characterized ZnPC@MIL-101, demonstrating its potential as an effective agent for photodynamic therapy against MCF-7 breast cancer cells. The structural and photophysical characterization confirmed the successful integration of ZnPC into the MIL-101 framework, with consequent impacts on the material's surface area, pore size, and morphology, suggestive of efficient photosensitizer loading. The cellular studies highlighted the statistically significant synergistic effect of ZnPC@MIL-101 and laser radiation in reducing the viability of MCF-7 cells, showcasing the composite's potential for targeted cancer treatment via PDT. These findings pave the way for further exploration of ZnPC@MIL-101 in various biomedical applications, highlighting the material's versatility and promising therapeutic potential, provided the acknowledged limitations are addressed in future research.

FUNDING

This research received no specific grant from any funding agency in the public, commercial, or not-for-profit sectors.

ETHICAL APPROVAL

For this type of study, ethical approval was not required.

CONFLICTS OF INTEREST

The authors have declared no conflict of interest.

CONSENT TO PARTICIPATE

Not applicable.

CONSENT FOR PUBLICATION

Not applicable.

AVAILABILITY OF DATA AND MATERIAL

Not applicable.

AUTHOR CONTRIBUTIONS

M. V: Data curation, Formal analysis, Investigation, Methodology, Software, and Writing an original draft. **Z.S:** Data curation, Formal analysis, Investigation, Methodology, Software, and Writing-Review & Editing. **R.R:** Data curation, Formal analysis, Investigation, Software, and Writing-Review & Editing. **M.S.:** Data curation and Formal analysis. **H.N:** Data curation and Formal analysis. **S.H.G:** Data curation, Formal analysis, and Writing-Review & Editing. **A.H:** Data curation, Formal analysis, and Writing-Review & Editing. **M.D:** Supervision, Project administration, and Writing-Review & Editing.

REFERENCES

1. Correia JH, Rodrigues JA, Pimenta S, Dong T, Yang Z. Photodynamic Therapy Review: Principles, Photosensitizers, Applications, and Future Directions. Pharmaceutics. 2021;13(9):1332.
2. Dougherty TJ, Gomer CJ, Henderson BW, Jori G, Kessel D, Korbelik M, et al. Photodynamic therapy. J Natl Cancer Inst. 1998;90(12):889-905.
3. Tunç T, Karakuş G, Sümer Z. Investigation of Cytotoxic and Antimicrobial Effects of Polyanhydride-Based Poly[(maleic anhydride)-co-(vinyl Acetate)] Conjugates Combined with Methotrexate and Gemcitabine in Breast Cancer Treatment. ACS Omega. 2025;10(12):12152-12162.
4. Khan SY, Bah T, Layeequr Rahman R. The Role of Molecular Profiling in De-Escalation of Toxic Therapy in Breast Cancer. Int J Mol Sci. 2025;26(3):1332.
5. Fakudze N, Abrahamse H, George B. Nanoparticles improved pheophorbide-a mediated photodynamic therapy for cancer. Lasers Med Sci. 2025;40(1): 1-8.
6. Erdemir GY, Kuruçay A, Ates B, Altundas A. Development of 1,2,3-Triazolopyridazinone Derivatives as Potential Caspase 3 and Apoptosis Inducers: Design, Synthesis and Anticancer Activity Studies. J Biochem Mol Toxicol. 2025;39(3):e70216.
7. Khosrojerdi S, Gholami L, Khazaei M, Hashemzadeh A, Darroudi M, Oskuee RK. Synthesis and evaluation of gene delivery vectors based on PEI-modified metal-organic framework (MOF) nanoparticles. Iran J Basic Med Sci. 2024;27(2):203.
8. Hashemzadeh A, Drummen GP, Avan A, Darroudi M, Khazaei M, Khajavian R, et al. When metal–organic framework–mediated smart drug delivery meets gastrointestinal cancers. J Mater Chem B 2021;9(19):3967-3982.
9. Xue Z, Zhu M, Dong Y, Feng T, Chen Z, Feng Y, et al. An integrated targeting drug delivery system based

on the hybridization of graphdiyne and MOFs for visualized cancer therapy. Nanoscale. 2019;11(24):11709-11718.
10. Li B, Ashrafizadeh M, Jiao T. Biomedical application of metal-organic frameworks (MOFs) in cancer therapy: Stimuli-responsive and biomimetic nanocomposites in targeted delivery, phototherapy and diagnosis. Int J Biol Macromol. 2024; 260:129391.
11. Shaabani A, Sepahvand H, Amini MM, Hashemzadeh A, Boroujeni MB, Badali E. Tandem oxidative isocyanide-based cycloaddition reactions in the presence of MIL-101 (Cr) as a reusable solid catalyst. Tetrahedron. 2018;74(15):1832-1837.
12. Boroujeni MB, Hashemzadeh A, Faroughi M-T, Shaabani A, Amini MM. Magnetic MIL-101-SO 3 H: a highly efficient bifunctional nanocatalyst for the synthesis of 1, 3, 5-triarylbenzenes and 2, 4, 6-triaryl pyridines. RSC advances. 2016;6(102):100195-100202.
13. Kocaağa N, Türkkol A, Bilgin MD, Erdoğmuş A. The synthesis of novel water-soluble zinc (II) phthalocyanine based photosensitizers and exploring of photodynamic therapy activities on the PC3 cancer cell line. Photochem Photobiol Sci. 2023;22(9):2037-2053.
14. Halkiotis KN, Uzunoglu NK, Loukas S, Pantelias GE, Trafalis D, Yova D, editors. Influence of drug and light dose in determining PDT efficacy in human pancreatic cancer cells, treated with zinc tetrasulfonated phthalocyanines (ZnTSPc). Proc SPIE-Int Soc Opt Eng. 1997;3191:243-252.
15. Feuser PE, Cordeiro AP, de Bem Silveira G, Borges Corrêa MEA, Lock Silveira PC, Sayer C, et al. Co-encapsulation of sodium diethyldithiocarbamate (DETC) and zinc phthalocyanine (ZnPc) in liposomes promotes increases phototoxic activity against (MDA-MB 231) human breast cancer cells. Colloids Surf B. 2021;197:111434.
16. Wysocki M, Ziental D, Biyiklioglu Z, Jozkowiak M, Baş H, Dlugaszewska J, et al. Non-peripheral octasubstituted zinc(II) phthalocyanines bearing pyridinepropoxy substituents – Antibacterial, anticancer photodynamic and sonodynamic activity. J Inorg Biochem. 2025;262:112751.
17. Demirbaş Ü, Pişkin M, Durmuş M, Kantekin H. Metal or metal-free phthalocyanines containing morpholine substituents: synthesis, spectroscopic and photophysicochemical properties. J Coord Chem. 2022;75(9-10):1243-1255.
18. Roguin LP, Chiarante N, García Vior MC, Marino J. Zinc(II) phthalocyanines as photosensitizers for antitumor photodynamic therapy. Int J Biochem Cell Biol. 2019;114:105575.
19. Nash GT, Luo T, Lan G, Ni K, Kaufmann M, Lin W. Nanoscale Metal-Organic Layer Isolates Phthalocyanines for Efficient Mitochondria-Targeted Photodynamic Therapy. J Am Chem Soc. 2021;143(5):2194-2199.
20. Yang Z, Li P, Chen Y, Dong E, Feng Z, He Z, et al. Preparation of zinc phthalocyanine-loaded amphiphilic phosphonium chitosan nanomicelles for enhancement of photodynamic therapy efficacy. Colloids Surf B. 2021;202:111693.
21. Kong J, Cai M, Zhu R, Zhang Y, Du Y, Jing X, et al. The utilization of metal-organic frameworks in tumor-targeted drug delivery systems. J Sci: Adv Mater Devices. 2024;9(3):100770.
22. Luo T, Nash GT, Xu Z, Jiang X, Liu J, Lin W. Nanoscale Metal-Organic Framework Confines Zinc-Phthalocyanine Photosensitizers for Enhanced Photodynamic Therapy. J Am Chem Soc. 2021;143(34):13519-13524.
23. Liu J, Kang DW, Fan Y, Nash GT, Jiang X, Weichselbaum RR, et al. Nanoscale Covalent Organic Framework with Staggered Stacking of Phthalocyanines for Mitochondria-Targeted Photodynamic Therapy. J Am Chem Soc. 2024;146(1):849-857.
24. Mhettar P, Kale N, Pantwalawalkar J, Nangare S, Jadhav N. Metal-organic frameworks: Drug delivery applications and future prospects. Admet dmpk. 2024;12(1):27-62.
25. Li D, Cai S, Wang P, Cheng H, Cheng B, Zhang Y, et al. Innovative Design Strategies Advance Biomedical Applications of Phthalocyanines. Adv Healthc Mater. 2023;12(22):2300263.
26. Ye Y, Zhao Y, Sun Y, Cao J. Recent Progress of Metal-Organic Framework-Based Photodynamic Therapy for Cancer Treatment. Int J Nanomedicine. 2022;17:2367-2395.
27. Zhao W, Wang L, Zhang M, Liu Z, Wu C, Pan X, et al. Photodynamic therapy for cancer: mechanisms, photosensitizers, nanocarriers, and clinical studies. MedComm. 2024;5(7):e603.
28. Li M, Zhang Z, Yu Y, Yuan H, Nezamzadeh-Ejhieh A, Liu J, et al. Recent advances in Zn-MOFs and their derivatives for cancer therapeutic applications. Mater Adv. 2023;4(21):5050-5093.
29. Zhong YT, Cen Y, Xu L, Li SY, Cheng H. Recent Progress in Carrier-Free Nanomedicine for Tumor Phototherapy. Adv Healthc Mater. 2023;12(4):2202307.
30. Sun J, Zhang X, Zhang D, Chen YP, Wang F, Li L, et al. Building Block Symmetry Relegation Induces Mesopore and Abundant Open-Metal Sites in Metal-Organic Frameworks for Cancer Therapy. CCS Chem. 2022;4(3):996-1006.
31. Kalhori F, Yazdyani H, Khademorezaeian F, Hamzkanloo N, Mokaberi P, Hosseini S, et al. Enzyme activity inhibition properties of new cellulose nanocrystals from Citrus medica L. pericarp: A perspective of cholesterol lowering. Luminescence. 2022;37(11):1836-1845.
32. Ghoochani SH, Hosseini HA, Sabouri Z, Soheilifar MH, Neghab HK, Hashemzadeh A, et al. Zn(II) porphyrin–encapsulated MIL-101 for photodynamic therapy of breast cancer cells. Lasers Med Sci. 2023;38(1):151.
33. Chota A, Abrahamse H, George BP. Green synthesis and characterization of AgNPs, liposomal loaded AgNPs, and ZnPcS4 photosensitizer for enhanced photodynamic therapy effects in MCF-7 breast

cancer cells. Photodiagn Photodyn Ther. 2024;48:104252.
34. Chota A, Abrahamse H, George BP. Chemotoxic and phototoxic effects of liposomal co-delivery of green synthesized silver nanoparticles and ZnPcS4 for enhanced photodynamic therapy in MCF-7 breast cancer cells: An in vitro study. Biomed Pharmacother. 2025;185:117986.
35. Larroque C, Pelegrin A, Van Lier JE. Serum albumin as a vehicle for zinc phthalocyanine: Photodynamic activities in solid tumour models. BR J CANCER. 1996;74(12):1886-1890.
36. Hashemzadeh A, Amini MM, Tayebee R, Sadeghian A, Durndell LJ, Isaacs MA, et al. A magnetically-separable $H_3PW_{12}O_{40}$@ Fe_3O_4/EN-MIL-101 catalyst for the one-pot solventless synthesis of 2H-indazolo [2, 1-b] phthalazine-triones. Mol Catal. 2017;440:96-106.
37. Yeganeh AD, Amini MM, Safari N. In situ synthesis and encapsulation of copper phthalocyanine into MIL-101 (Cr) and MIL-100 (Fe) pores and investigation of their catalytic performance in the epoxidation of styrene. J Porphyrins Phthalocyanines. 2019;23(10):1118-1131.
38. Manoto SL, Houreld N, Hodgkinson N, Abrahamse H. Modes of Cell Death Induced by Photodynamic Therapy Using Zinc Phthalocyanine in Lung Cancer Cells Grown as a Monolayer and Three-Dimensional Multicellular Spheroids. Molecules. 2017;22(5):791.
39. Xu D, You Y, Zeng F, Wang Y, Liang C, Feng H, et al. Disassembly of Hydrophobic Photosensitizer by Biodegradable Zeolitic Imidazolate Framework-8 for Photodynamic Cancer Therapy. ACS Appl Mater Interfaces. 2018;10(18):15517-15523.
40. Ben-Hur E, Chan WS. Phthalocyanines in Photobiology and Their Medical Applications. The Porphyrin Handbook: Multporphyrins, Multiphthalocyanines and Arrays. 2012;19:1-35.
41. Ramya E, Momen N, Desai N. Preparation of Multiwall Carbon Nanotubes with Zinc Phthalocyanine Hybrid Materials and Their Nonlinear Optical (NLO) Properties. J Nanosci Nanotechnol. 2018;18:4764-4770.
42. Pişkin M. The novel 2,6-dimethoxyphenoxy substituted phthalocyanine dyes having high singlet oxygen quantum yields. Polyhedron. 2016;104:17-24.
43. Guo S, Gu D, Yang Y, Tian J, Chen X. Near-infrared photodynamic and photothermal co-therapy based on organic small molecular dyes. J Nanobiotechnol. 2023;21(1):348.
44. Tu J, Wang T, Shi W, Wu G, Tian X, Wang Y, et al. Multifunctional ZnPc-loaded mesoporous silica nanoparticles for enhancement of photodynamic therapy efficacy by endolysosomal escape. Biomaterials. 2012;33:7903-7914.
45. Borzęcka W, Domiński A, Kowalczuk M. Recent Progress in Phthalocyanine-Polymeric Nanoparticle Delivery Systems for Cancer Photodynamic Therapy. Nanomaterials. 2021;11(9):2426.
46. Zhou Z, Song J, Nie L, Chen X. Reactive oxygen species generating systems meeting challenges of photodynamic cancer therapy. Chem Soc Rev. 2016;45(23):6597-6626.
47. Roguin LP, Chiarante N, García Vior MC, Marino J. Zinc(II) phthalocyanines as photosensitizers for antitumor photodynamic therapy. Int J Biochem Cell Biol. 2019;114:105575.
48. Yan S, Guo H, Su J, Chen J, Song X, Huang M, et al. Effects of hydroxyl radicals produced by a zinc phthalocyanine photosensitizer on tumor DNA. Dyes Pigm. 2020;173:107894.
49. Çakir V, Çakir D, Pişkin M, Durmuş M, Biyiklioğlu Z. Water soluble peripheral and non-peripheral tetrasubstituted zinc phthalocyanines: Synthesis, photochemistry and bovine serum albumin binding behavior. J Lumin. 2014;154:274-284.
50. Li R, Zheng K, Hu P, Chen Z, Zhou S, Chen J, et al. A novel tumor targeting drug carrier for optical imaging and therapy. Theranostics. 2014;4(6):642-659.
51. Obata M, Ishihara E, Hirohara S. Effect of tertiary amino groups in the hydrophobic segment of an amphiphilic block copolymer on zinc phthalocyanine encapsulation and photodynamic activity. RSC Adv. 2022;12(28):18144-18153.
52. Zha Z, Miao Y, Huiling T, Herrera-Balandrano D, Yin H, Wang S. Heparosan-based self-assembled nanocarrier for zinc(II) phthalocyanine for use in photodynamic cancer therapy. Int J Biol Macromol. 2022;219:31-43
53. Tong L, Zhang S, Huang R, Yi H, Wang J-W. Extracellular vesicles as a novel photosensitive drug delivery system for enhanced photodynamic therapy. Front Bioeng Biotechnol. 2022;10:1032318.
54. Udrea AM, Smarandache A, Dinache A, Mares C, Nistorescu S, Avram S, et al. Photosensitizers-Loaded Nanocarriers for Enhancement of Photodynamic Therapy in Melanoma Treatment. Pharmaceutics. 2023;15(8):2124.
55. Shaabani A, Mohammadian R, Hashemzadeh A, Afshari R, Amini MM. Amine-functionalized MIL-101 (Cr) embedded with Co (ii) phthalocyanine as a durable catalyst for one-pot tandem oxidative A 3 coupling reactions of alcohols. New J Chem. 2018;42(6):4167-4174.
56. Mantareva V, Iliev I, Sulikovska I, Durmuş M, Angelov I. Cobalamin (Vitamin B12) in Anticancer Photodynamic Therapy with Zn(II) Phthalocyanines. Int J Mol Sci. 2023;24(5): 4400.
57. Ma C, Wang Y, Chen W, Hou T, Zhang H, Zhang H, et al. Caspase-1 Regulates the Apoptosis and Pyroptosis Induced by Phthalocyanine Zinc-Mediated Photodynamic Therapy in Breast Cancer MCF-7 Cells. Molecules. 2023;28(16): 5934.
58. Ahmetali E, Sen P, Süer NC, Nyokong T, Eren T, Şener MK. Photodynamic therapy activities of phthalocyanine-based macromolecular photosensitizers on MCF-7 breast cancer cells. J Macromol Sci Part A Pure Appl Chem. 2021;58(11):748-757.
59. Yan S, Dong L, Hu Z, Zhang Y, Xu W, Xing J, et al. A Photosensitizer-Loaded Polydopamine Nanomedicine Agent for Synergistic Photodynamic

and Photothermal Therapy. Molecules. 2023;28(15): 5874.
60. Oshiro-Junior JA, Sato MR, Boni FI, Santos KLM, de Oliveira KT, de Freitas LM, et al. Phthalocyanine-loaded nanostructured lipid carriers functionalized with folic acid for photodynamic therapy. Mater Sci Eng C. 2020;108:110462.
61. Mfouo-Tynga I, Houreld NN, Abrahamse H. Induced cell death pathway post photodynamic therapy using a metallophthalocyanine photosensitizer in breast cancer cells. Photomed Laser Surg. 2014;32(4):205-211.
62. Valli F, García Vior MC, Roguin LP, Marino J. Crosstalk between oxidative stress-induced apoptotic and autophagic signaling pathways in Zn(II) phthalocyanine photodynamic therapy of melanoma. Free Radic Biol Med. 2020;152:743-754.
63. Malek-Esfandiari Z, Rezvani-Noghani A, Sohrabi T, Mokaberi P, Amiri-Tehranizadeh Z, Chamani J. Molecular dynamics and multi-spectroscopic of the interaction behavior between bladder cancer cells and calf thymus DNA with rebeccamycin: apoptosis through the down regulation of PI3K/AKT signaling pathway. J Fluoresc. 2023;33(4):1537-1557.
64. Aydogdu S, Yasa Atmaca G, Erdoğmuş A, Hatipoglu A. Synthesis of a new Zn-phthalocyanine, photophysical, photochemical, and sono-photochemical properties and DFT studies. Polyhedron. 2024;256:116989.